Magnetohydrodynamic stratified bioconvective flow of micropolar nanofluid due to gyrotactic microorganisms

Cite as: AIP Advances **9**, 025208 (2019); https://doi.org/10.1063/1.5085742
Submitted: 14 December 2018 • Accepted: 01 February 2019 • Published Online: 13 February 2019

S. M. Atif, S. Hussain and M. Sagheer

Magnetohydrodynamic stratified bioconvective flow of micropolar nanofluid due to gyrotactic microorganisms

Cite as: AIP Advances 9, 025208 (2019); doi: 10.1063/1.5085742
Submitted: 14 December 2018 • Accepted: 1 February 2019 •
Published Online: 13 February 2019

S. M. Atif,[a] S. Hussain, and M. Sagheer

AFFILIATIONS

Department of Mathematics, Capital University of Science and Technology, 44000 Islamabad, Pakistan

[a]Corresponding author e-mail address: dmt161001@cust.pk.

ABSTRACT

The forthright purpose of this communication is to inspect the flow of magnetohydrodynamic (MHD) stratified micropolar bioconvective fluid containing nanoparticles and gyrotactic microorganism. The phenomenon of thermal radiation and Joule heating has also been incorporated. In order to stabilize the suspended nanoparticles, bioconvection which is established by the combined effects of magnetic field and buoyancy force is implemented. A system of PDEs is converted into the ODEs by invoking the appropriate similarity transformation and the transformed equations are then solved by the well known shooting technique. The interesting aspects of sundry parameters on the velocity, the angular velocities, the temperature, concentration and the motile microorganism density are examined and sketched. The skin friction and the couple stress coefficients, the heat and mass transfer rates and the local density number of the motile microorganism have been numerically computed and discussed. Our analysis depicts that the temperature, concentration and motile microorganism density depreciate for the increment in the material parameter. An enhancement in the buoyancy ratio parameter results an enhancement in the energy and the motile microorganism density profile whereas the velocity profile is reduced.

I. INTRODUCTION

The study of magnetohydrodynamics (MHD) plays a vital role due to its importance in industry and many other flow phenomenon. It has applications in many fields for example, fluid dynamics, metallurgical science, aerodynamics, mental working processes, and many engineering disciplines such as biomedical engineering, composite or ceramic engineering and heat exchangers etc. The objective of the induction of MHD is to modify the flow fields in a preferred direction by varying the structure of the boundary layer. In convection processes, such as metal casting, control reactor in nuclear reactors and material manufacturing fields application of the magnetic field also plays a significant role. Zheng *et al.*[1] ascertained the heat transfer of two dimensional MHD flow over a porous surface with velocity slip and temperature jump. It was noticed that the thermal boundary layer hiked due to an enhancement in the shrinking parameter. Chauhan and Agrawal[2] reported the MHD flow and heat transfer in a channel bounded by shrinking sheet and porous bed with the main observation that the magnetic number and suction parameter controls the cooling rate. Attia[3] considered the variable physical properties to analyze the transfer of heat in an unsteady MHD Couette flow in dusty fluid with a major finding that temperature of both fluid and dust particles significantly changed. Kumar *et al.*[4] presented the heat and mass transfer of radiative MHD mixed convection Casson fluid flow with cross diffusion effect over a vertical plate. It was concluded that an acclivity in the mixed convection parameter and the buoyancy force parameter enrich the fluid motion.

Micropolar fluids are characterized as the fluids having micro structures. Analysis of the micropolar fluids has been an active field of interest for many researchers. Eringen[5,6]

highlighted and developed the applications of micropolar theory to attract the attention of many researchers towards the micropolar fluids. Soundalgekar and Takhar[7] studied the micropolar fluid and found that the growing values of the coupling constant causes an enhancement in the micro-rotation distribution. Eldabe and Ouaf[8] explored the heat transfer in the hydromagnetic flow of the micropolar fluid with the viscous dissipation and Ohmic effect past a stretching sheet by using the Chebyshev finite difference method and noticed that the thermal profile was reduced as the Prandtl number gets higher whereas there was a reverse effect for the growing values of the Eckert number. By considering the porous stretching sheet, Motsa and Shateyi[9] studied the MHD micropolar fluid with the chemical reaction, Hall ion-slip current and the thermal diffusivity. It was concluded that the velocity profile enhances with gradually increasing values of the Hall current. Bilal *et al.*[10] reported the magneto micropolar nanofluid using the variable thermal diffusivity, Hall and ion-slip effects. An increment in the thermal radiation was found to decline in the fluid motion. By considering the viscous effects, Hsiao[11] obtained the solution of the magnetohydrodynamic micropolar nanofluid flow towards a stretching sheet and observed that the rate of heat transfer was enhanced as either of the Prandtl and Eckert numbers were increased. Atif *et al.*[12] ascertained the MHD micropolar Carreau nanofluid in the presence of induced magnetic field and reported that the angular velocity upsurges with an augmentation in the magnetic Prandtl number and the material parameter.

The enhancement of the heat transfer is one of the main concerns of the researchers. In this regard, the nanofluids are of great interest for the community. On comparing the nanofluids with the base fluids such as mineral oils, ethylene glycol and water nanofluids have the tendency to improve the thermophysical properties. Nanoparticles have very useful characteristic of passing through the microchannels and capillaries without creating any blockage in the flow. Choi[13] experimentally verified that the addition of the nano-sized particles in the base fluid, the thermal properties can be enhanced. Rashidi *et al.*[14] reviewed the generalized magnetic field effects in Burger's nanofluid and reported that the momentum boundary layer thickness reduces for Burger's model due to the extra viscoelastic effects. Feng and Kleinstreuer[15] considered the parallel disks system and discussed the nanofluid convective heat transfer. Their main concluding observation was that a higher nanoparticles volume fraction, large inlet Reynolds number, reduced disk spacing and the smaller nanoparticle diameter, augments the Nusselt number. Over an isothermal flat plate Reddy *et al.*[16] recently investigated the entropy generation in colloidal study of unsteady magnetohydrodynamic couple stress fluid. They reported that the entropy generation is upsurged with an increment in the Grashof parameters but declined as the couple stress or the magnetic number is increased. Enhanced electroosmotic flow in a nano-channel was analyzed by Bhattacharyya and Pala.[17] The concluding result of that study was that an increasing the span ratio between the no-slip and slip regions causes an augmentation in the average electroosmotic flow.

Phenomenon due to the upward swimming of the microorganisms is called bioconvection. Upward motion of these microorganisms tends to concentrate in the upper portion of the fluid which becomes unstable due to heavy density stratification. Motile micro-organisms are self-propelled and by swimming in a specific direction in the base fluid, these microorganism increase the density of the base fluid in response to some stimulant. Microorganisms may be oxytaxis, gyrotaxis or gravitaxis organisms. Unlike the motile microorganisms, the nanoparticles are not self-propelled, and their motion is driven by Brownian motion and thermophoresis occurring in the nanofluid. Thus, the motion of the motile microorganisms is independent of the motion of nanoparticles. There addition in the nanofluid is to enhance the stability of the suspensions. Kuznetsov[18–20] was the first who presented the idea of the nanofluid bioconvection and also investigated the impact of the gyrotactic microorganism on the nanofluids. Kuznetsov[19] observed that in a horizontal layer of nanofluid containing gyrotactic microorganisms, the nanoparticles may either elevate or depress critical Rayleigh numbers, whereas the microorganisms have a consistently destabilizing effect. By considering oxytactic motile microorganism, bioconvection in nanofluid saturated in a porous media, he also identified that the nanofluid stability is dictated by nanoparticles distribution, density stratification induced by the vertical temperature gradient and also the density stratification induced by up-swimming of oxytactic microorganisms.[20] This study has further shown that the presence of oxytactic microorganisms decreases the nanofluid suspension stability and eliminates oscillatory instability rather than non-oscillatory instability. Xu and Pop[21] studied the mixed convection flow of a nanofluid containing gyrotactic microorganisms in a horizontal channel and concluded that the motile density is decreased as the Schmidt number is increased for the positive Reynolds number. Raju and Sandeep[22] studied the bioconvection in MHD non-Newtonian fluid flow with cross diffusion past a rotating plate and a rotating cone and found that the rotating cone has significantly better heat and mass transfer. Wang and Fan[23] ascertained that the nanoparticles are of four scales: the mega scale, the molecular scale, the macro scale and the micro scale. The motion of the gyrotactic microorganism is microscopic (convection) and the bioconvection process is a mega scale phenomenon. Ramya and Doh[24] ascertained the hydrodynamic effect of the absorbing/emitting radiation on the micropolar liquid containing the gyrostatic microorganisms and investigated that the motile microorganisms density was enhanced as the bioconvection Lewis number is increased for both moving and the fixed plate case. The effect of the thermal radiation is discussed by many authors.[25–27]

The present article focused on the detailed analysis of the radiative MHD micropolar nanofluid containing gyrotactic microorganisms with stratification effects. The arising ODEs for the problem are solved via well known shooting technique. The demeanor of all the emerging physical parameters are displayed graphically with an appropriate discussion.

II. PROBLEM FORMULATION

An incompressible, two dimensional mixed convection electrically conducting micropolar nanofluid past a stretching sheet has been considered for analysis. The stratification, Joule heating and thermal radiation effects have also been incorporated. The microorganisms are induced to stabilize the nanoparticles. The velocity and swimming direction of these microorganism is not effected by the nanoparticles. The cartesian coordinate system is taken in such a way that the horizontal axis is chosen in the direction of the stretching sheet with stretching velocity $u = ax$ and vertical axis is normal to the stretching surface. The flow is restricted in the region $y > 0$. A uniform magnetic field of strength B_0 is applied in the positive $y-axis$ direction. A magnetic Reynolds number is assumed to be very small such that the induced magnetic field is neglected. The physical layout of the modeled problem is illustrated in Fig. 1.

Subject to above mentioned constraints, the governing equations are expressed as follows:

Continuity equation

$$\frac{\partial v}{\partial y} + \frac{\partial u}{\partial x} = 0, \tag{1}$$

Momentum equation

$$u\frac{\partial u}{\partial x} + v\frac{\partial u}{\partial y} = \left(\nu_f + \frac{k_f}{\rho_f}\right)\frac{\partial^2 u}{\partial y^2} + \frac{k_f}{\rho_f}\frac{\partial N}{\partial y} - \frac{1}{\rho_f}\sigma B_0^2 u + \frac{1}{\rho_f}\left[(1-C_f)\rho_f\beta g(T-T_\infty) - g(\rho_p - \rho_f)(C-C_f) - \gamma^* g(n-n_\infty)(\rho_m - \rho_f)\right], \tag{2}$$

Angular momentum equation

$$u\frac{\partial N}{\partial x} + v\frac{\partial N}{\partial y} = \frac{\gamma_f}{(\rho j)_f}\frac{\partial}{\partial y}\left(\frac{\partial N}{\partial y}\right) - \frac{k_f}{(\rho j)_f}\left(2N + \frac{\partial u}{\partial y}\right), \tag{3}$$

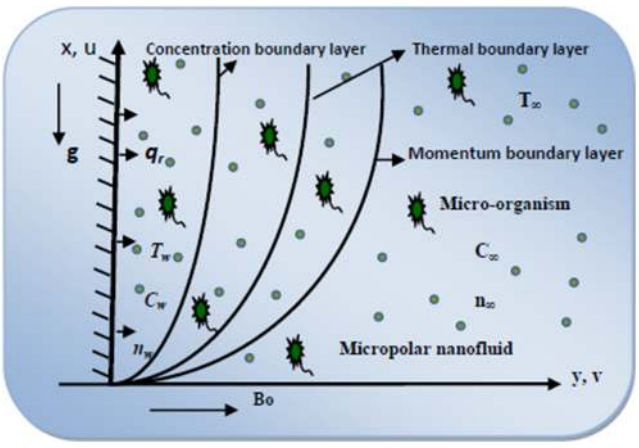

FIG. 1. Flow configuration.

Energy equation

$$u\frac{\partial T}{\partial x} + v\frac{\partial T}{\partial y} = \alpha\frac{\partial}{\partial y}\left(\frac{\partial T}{\partial y}\right) + \frac{Q_0}{(\rho C_p)_f}(T-T_\infty) - \frac{1}{(\rho C_p)_f}\frac{\partial q_r}{\partial y} + \frac{\sigma B_0^2}{(\rho C_p)_f}u^2 + \tau\left[D_B\frac{\partial C}{\partial y}\frac{\partial T}{\partial y} + \frac{D_T}{T_\infty}\left(\frac{\partial T}{\partial y}\right)\left(\frac{\partial T}{\partial y}\right)\right], \tag{4}$$

Nanoparticles concentration equation

$$u\frac{\partial C}{\partial x} + v\frac{\partial C}{\partial y} = \frac{D_T}{T_\infty}\frac{\partial}{\partial y}\left(\frac{\partial T}{\partial y}\right) + D_B\frac{\partial}{\partial y}\left(\frac{\partial C}{\partial y}\right), \tag{5}$$

Density of gyrotactic microorganism

$$u\frac{\partial n}{\partial x} + v\frac{\partial n}{\partial y} + bW_c\frac{\partial}{\partial y}\left(\frac{n}{\Delta C}\frac{\partial C}{\partial y}\right) = D_m\left(\frac{\partial^2 n}{\partial y^2}\right). \tag{6}$$

The considered boundary conditions for the above problem are:

$$\left.\begin{aligned} &u_w = ax,\ v = 0,\ N = 0,\ T = T_w = T_0 + b_1 x,\\ &C = C_w = C_0 + d_1 x, \qquad n = n_w = n_0 + e_1 x \end{aligned}\right\} \quad \text{at} \quad y = 0,$$
$$\left.\begin{aligned} &u \to 0, \qquad N \to 0, \qquad T = T_\infty = T_0 + b_2 x,\\ &C = C_\infty = C_0 + d_2 x, \qquad n = n_\infty = n_0 + e_2 x \end{aligned}\right\} \quad \text{as} \quad y \to \infty \tag{7}$$

In the above expressions σ represents the electrical conductivity, β the volume expansion coefficient, B_0 the magnetic field intensity, g is the gravity, α thermal diusivity, ρ_f, ρ_p and ρ_m represents the nanofluid density, nanoparticles density and microorganism particle density respectively. The temperature, concentration of nanoparticles and concentration of the microorganisms are presented by T, C and n respectively. The reference temperature, reference concentration of nanoparticles and reference concentration of the microorganisms are denoted by T_0, C_0 and n_0 respectively. The surface temperature, surface concentration of nanoparticles, surface concentration of the microorganisms, the ambient temperature, ambient concentration of nanoparticles and ambient concentration of the microorganisms are represented by T_w, C_w, n_w, T_∞, C_∞ and n_∞ respectively, N denotes the microrotation or the angular velocity, C_p the specific heat, b_1, b_2, c_1, c_2, e_1 and e_2 are the dimensionless constants.

In (3), the spin gradient viscosity γ_f, is given by

$$\gamma_f = \left(\mu_f + \frac{k_f}{2}\right)j.$$

where $j = \nu_f/a$ is the micro-inertia density and k_f is the vortex viscosity. In equation (4), q_r is the Rosseland radiative heat flux and is defined as

$$q_r = -\frac{4\sigma^*}{3\kappa^*}\frac{\partial T^4}{\partial y}.$$

where σ^* the Stefan-Boltzmann constant and κ^* is the mean absorption coefficients. By using Taylor series and expanding T^4 about the ambient fluid temperature T_∞, we have

$$T^4 = T_\infty^4 + 4T_\infty^3(T-T_\infty) + 6T_\infty^2(T-T_\infty)^2 + \ldots\ldots$$

In equation (6), n represents the motile density of microorganisms, b is the chemotaxis constant, $\frac{bW_c}{\Delta C}\nabla C$ is the velocity related to cell swimming, W_c is the maximum cell swimming speed and D_m the microorganisms diffusion coefficient.

By using the following transformation,[11] equations (2)–(6) are transformed into the system of ordinary differential equations.

$$\left.\begin{aligned} &\eta = y\sqrt{\frac{a}{\nu_f}},\ u = axf'(\eta),\ v = -f(\eta)\sqrt{a\nu_f},\ N = ax\sqrt{\frac{a}{\nu_f}}g(\eta),\\ &\theta(\eta) = \frac{T - T_\infty}{T_w - T_0}, \qquad \phi(\eta) = \frac{C - C_\infty}{C_w - C_0}, \qquad \xi(\eta) = \frac{n - n_\infty}{n_w - n_0}. \end{aligned}\right\} \tag{8}$$

As a result equation (1) is satisfied identically and equations (2)–(6) yield

$$(1+K)f''' - f'^2 + ff'' + Kg' - Mf' + \lambda(\theta - Nr\phi - Rb\epsilon) = 0, \tag{9}$$

$$\left(1+\frac{K}{2}\right)g'' - gf' + fg' - K(2g + f'') = 0. \tag{10}$$

$$\left.\begin{aligned} &\left(1+\frac{4}{3}Rd\right)\theta'' + Prf\theta' - Prf'\theta - Prf'S + Pr\delta\theta + PrMEcf'^2\\ &+ PrNb\theta'\phi' + PrNt\theta'^2 = 0, \end{aligned}\right\} \tag{11}$$

$$\phi'' + Sc(f\phi' - f'\phi - Qf') + \frac{Nt}{Nb}\theta'' = 0. \tag{12}$$

$$\xi'' - Lb(f'\xi - f\xi' + Bf') - Pe(\phi''(\xi + \Omega) + \xi'\phi') = 0. \tag{13}$$

The associated boundary conditions are:

$$\left.\begin{aligned} &f = 0,\ f' = 1,\ g = 0,\ \theta = 1 - S,\ \phi = 1 - Q,\ \xi = 1 - B \quad \text{at} \quad \eta = 0,\\ &f' \to 0,\ g \to 0,\ \theta \to 0,\ \phi \to 0,\ \xi \to 0 \quad \text{as} \quad \eta \to \infty. \end{aligned}\right\} \tag{14}$$

In the above equations, Pr denotes the Prandtl number, Pe the bioconvection Peclet number, λ the mixed convection parameter, G_r the Grashof number, Re_x the Reynolds number, K the micropolar constant, Ec the Eckert number, Ω the microorganism concentration difference parameter, M the magnetic number, B the motile density stratification, Lb the bioconvection Lewis parameter, S the thermal stratification parameter, Nb the Brownian motion parameter, Nt the thermophoresis parameter, Sc the Schmidt number, δ the heat generation coefficient, Rd the thermal radiation parameter, Rb the Rayleigh number, Q the mass stratification parameter and Nr the buoyancy ratio parameter. These parameters are formulated as:

$$Pr = \frac{\nu_f}{\alpha},\ Pe = \frac{bW_c}{D_m},\ \lambda = \frac{Gr}{Re_x^2},\ G_r = \frac{\beta g(1 - C_\infty)\Delta x^3}{\nu_f^2},\ Re_x = \frac{ax^2}{\nu_f},\ K = \frac{k_f}{\mu_f},$$

$$Ec = \frac{a^2x^2}{(C_p)_f(T_w - T_\infty)},\ \Omega = \frac{n_\infty}{n_w - n_0},\ M = \frac{\sigma B_0^2}{a\rho_f},\ B = \frac{e_2}{e_1},\ Lb = \frac{\nu_f}{D_m},\ S = \frac{b_2}{b_1},$$

$$Nb = \frac{(\rho C_p)_p D_B(C_w - C_\infty)}{(\rho C_p)_f \nu_f},\ Nt = \frac{(\rho C_p)_p D_T(T_w - T_\infty)}{(\rho C_p)_f T_\infty \nu_f},\ Sc = \frac{\nu_f}{D_B},\ \delta = \frac{Q_0}{a(\rho C_p)_f},$$

$$Rd = \frac{4\sigma^* T_\infty^3}{k\kappa^*},\ Rb = \frac{\gamma(n_w - n_0)(\rho_m - \rho_f)}{\beta\rho_f(1 - C_\infty)(T_w - T_0)},\ Q = \frac{d_2}{d_1},\ Nr = \frac{(\rho_p - \rho_f)(C_w - C_0)}{\beta\rho_f(T_w - T_0)},$$

A. Quantities of interest

The physical quantities of foremost interest are the skin friction coefficient, the Nusselt number, the Sherwood number and the density number of the motile microorganisms. These dimensionless quantities are defined as:

$$C_f = \frac{\tau_w}{\rho_f u_w^2}, \qquad Nu_x = \frac{xq_w}{k(T_w - T_0)},$$

$$Sh_x = \frac{xq_m}{D_B(C_w - C_0)}, \qquad Nn_x = \frac{xq_n}{D_n(n_w - n_0)}.$$

For this problem, the quantities τ_w, q_x, q_m and q_n are defined as

$$\tau_w = \mu\left[(1+\mathrm{K})\frac{\partial u}{\partial y}\right]_{y=0}, \qquad q_m = -\mathrm{D_B}\left(\frac{\partial C}{\partial y}\right)_{y=0},$$

$$q_w = -k\left[\left(1+\frac{16\sigma^*\mathrm{T}_\infty}{3k\kappa^*}\right)\frac{\partial T}{\partial y}\right]_{y=0}, \quad q_n = -\mathrm{D}_n\left(\frac{\partial \xi}{\partial y}\right)_{y=0}.$$

In dimensionless form

$$\left.\begin{aligned} C_f \mathrm{Re}_x^{1/2} &= (1+\mathrm{K})f''(0), & \mathrm{Sh}_x \mathrm{Re}_x^{-1/2} &= -\phi'(0), \\ \mathrm{Nu}_x \mathrm{Re}_x^{-1/2} &= -\left(1+\frac{4}{3}\mathrm{Rd}\right)\theta'(0), & \mathrm{Nn}_x \mathrm{Re}_x^{-1/2} &= -\xi'(0), \end{aligned}\right\} \tag{15}$$

where $\mathrm{Re}_x = \frac{ax^2}{\nu_f}$.

III. IMPLEMENTATION OF METHOD

The system of ODEs (9)–(13) subject to the boundary conditions (14) is solved numerically by using the shooting method.[28] For the conversion of the (9)–(13) into a system of the first order ODEs, introduce the new variables, $f = y_1, f' = y_2$, $f'' = y_3$, $g = y_4$, $g' = y_5$, $\theta = y_6$, $\theta' = y_7$, $\phi = y_8$, $\phi' = y_9$, $\xi = y_{10}$ and $\xi' = y_{11}$ to have the following set of eleven first order ordinary differential equations:

$$\left.\begin{aligned} y_1' &= y_2, \\ y_2' &= y_3, \\ y_3' &= \frac{1}{1+\mathrm{K}}\left[y_2^2 - y_1y_3 - \mathrm{K}y_5 + \mathrm{M}y_2 - \lambda(y_6 - \mathrm{N}ry_8 - \mathrm{R}by_{10})\right], \\ y_4' &= y_5, \\ y_5' &= \frac{2}{2+\mathrm{K}}\left[y_2y_4 - y_1y_5 + \mathrm{K}(2y_4 + y_3)\right], \\ y_6' &= y_7, \\ y_7' &= \frac{3\mathrm{P}r}{3+4\mathrm{Rd}}\left[y_2y_6 - y_1y_7 + \mathrm{S}y_2 - \delta y_6 - \mathrm{MEc}y_2^2 - \mathrm{N}by_7y_9 - \mathrm{N}ty_7^2\right], \\ y_8' &= y_9, \\ y_9' &= \mathrm{Sc}(y_2y_8 - y_1y_9 + \mathrm{Q}y_2) - \frac{\mathrm{N}t}{\mathrm{N}b}y_7', \\ y_{10}' &= y_{11}, \\ y_{11}' &= Lb(y_2y_{10} - y_1y_{11} + \mathrm{B}y_2) + Pe(y_9'(y_{10} + \Omega) + y_{11}y_9). \end{aligned}\right\} \tag{16}$$

The corresponding dimensionless boundary conditions are:

$$\left.\begin{aligned} &y_1 = 0, \quad y_2 = 1, \quad y_4 = 0, \quad y_6 = 1 - \mathrm{S}, \quad y_8 = 1 - \mathrm{Q}, \quad y_{10} = 1 - \mathrm{B} \quad \text{at } \eta = 0 \\ &y_2 \to 0, \quad y_4 \to 0, \quad y_6 \to 0, \quad y_8 \to 0, \quad y_{10} \to 0 \quad \text{as } \eta \to \infty. \end{aligned}\right\} \tag{17}$$

To solve the system of first order ordinary differential equations (16), with the help of the shooting method, eleven initial conditions are required. Therefore, we guess five unknown initial conditions $y_3(0) = p$, $y_5(0) = q$, $y_7(0) = r$, $y_9(0) = s$, $y_{11} = t$. The suitable guesses for five p, q, r, s and t unknown missing conditions are chosen such that the five known boundary conditions are approximately satisfied for $\eta \to \infty$. The Newton's iterative scheme is applied to improve the accuracy of the missing initial conditions p, q, r, s and t until the desired approximation is met. The computations have been performed for the various emerging parameters and for the appropriate bounded domain $[0, \eta_{max}]$ instead of $[0, \infty)$, where the positive real number η_{max} is chosen in such that no significant variations appeared in the results for the values greater than η_{max}. The stoping criteria for the iterative process is

$$\max\{|y_2(\eta_{max}) - 0|, |y_4(\eta_{max}) - 0|, |y_6(\eta_{max}) - 0|,$$
$$|y_8(\eta_{max}) - 0|, |y_{10}(\eta_{max}) - 0|\} < \zeta,$$

where ζ is a very small positive real number.

A. Validation of numerical scheme

For all the computations in the rest of this article, ζ has been chosen as 10^{-6}. For further reliability and validation

TABLE I. Comparison of the presently computed values of $-f''(0)$ and $g'(0)$ with those of Eldabe[8] and Hsiao.[11]

		$-f''(0)$			$g'(0)$		
M	K	8	11	Present	8	11	Present
0.0	0.2	0.9098	0.90976	0.909737	0.0950	0.09500	0.094997
0.5		1.1148	1.11437	1.114376	0.1051	0.10509	0.105090
1.0		1.2871	1.28711	1.287152	0.1121	0.11212	0.112061
	0	1.4142	1.41423	1.414216	0	0	0
	0.5	1.1408	1.14073	1.140786	0.2112	0.21116	0.211162
	2	0.7697	0.76958	0.769757	0.3586	0.35855	0.358664

of the code, the results of $-f''(0)$ and $g'(0)$ which were reported by Hsiao[8] and Eldabe,[11] are successfully reproduced and presented in Table I.

IV. RESULTS AND DISCUSSION

In this study, the impact of the various pertinent parameter on the skin friction coefficient, the microrotation parameter, the Nusselt, the Sherwood and local density numbers have been computed.

A. The skin friction coefficient and the microrotation parameter

Table II has presented to study the effects of sundry parameters on the skin friction coefficient and the microrotation parameter. It is observed that for the gradually boosting values of each of the micropolar parameter K, the magnetic number M, the buoyancy ratio parameter N*r* and the bioconvection Rayleigh number *Rb*, both the skin friction coefficient and the microrotation parameter are enhanced whereas with an increment in the mixed convection parameter λ, a reduction in the skin friction coefficient and the microrotation parameter is noticed.

B. The Nusselt number

Table III is prepared to analyze the impact of different involved parameters on the Nusselt number. It is noticed that due to an acclivity in each of the micropolar parameter K, the Prandtl number *Pr*, the mass stratification parameter Q and the thermal radiation parameter *Rd* the Nusselt number is increased. On the other hand the Nusselt number is reduced for an increment in each of the magnetic number M, the thermal stratification parameter S, the thermophoresis parameter Nt, the heat generation coefficient δ, the Eckert number *Ec*, the Brownian motion parameter N*b*.

TABLE II. Numerical values of the skin friction coefficient and the microrotation parameter for different parameters when *Pr* = *Pe* = *Lb* = 1.2, *Ec* = 0.02, *Rd* = 1, Ω = *Sc* = 0.2, *S* = *Q* = *B* = δ = *Nb* = *Nt* = 0.1.

K	M	λ	N*r*	*Rb*	$-C_f Re_x^{1/2}$	$g'(0)$
0.2	0.05	0.1	0.1	0.1	1.0736	0.1032
0.5					1.1926	0.2180
2					1.6197	0.5749
0.2	0				1.0468	0.1020
	0.5				1.2930	0.1128
	1				1.5025	0.1207
	0.05	0.1			1.0736	0.1032
		0.2			1.0302	0.1009
		0.3			0.9883	0.0988
		0.1	0.2		1.0845	0.1042
			0.4		1.1024	0.1056
			0.6		1.1204	0.1071
			0.1	0.2	1.0795	0.1036
				0.4	1.0870	0.1038
				0.6	1.0946	0.1041

TABLE III. Numerical values of the local Nusselt number for different parameters when *Pe* = *Lb* = 1.2, Ω = *Sc* = 0.2, λ = *Nr* = *B* = *Rb* = 0.1.

K	M	*Pr*	*Rd*	S	δ	*Ec*	*Nt*	*Nb*	Q	$Nu_x Re_x^{-1/2}$
0.2	0.05	1.2	1	0.1	0.1	0.02	0.1	0.1	0.1	1.3804
0.5										1.4285
2										1.5595
0.2	0									1.3934
	0.5									1.2765
	1									1.1836
	0.05	2								1.9114
		5								3.3285
		7								4.0218
		1.2	2							1.6409
			3							1.8720
			4							2.0910
			1	0.2						1.3266
				0.3						1.2724
				0.4						1.2177
				0.1	0.2					1.2666
					0.3					1.1351
					0.4					0.9780
					0.1	0.2				1.3756
						0.3				1.3730
						0.4				1.3704
						0.02	0.2			1.3647
							0.4			1.3337
							0.6			1.3032
							0.1	0.2		1.3656
								0.4		1.3336
								0.6		1.3016
								0.1	0.2	1.3825
									0.4	1.3867
									0.6	1.3908

C. The Sherwood number

The objective of the Table IV is to view the effect of different involved parameters on the local Sherwood number. It is evident from this table that an increment in the thermal stratification parameter S, the heat generation coefficient δ, the Eckert number *Ec*, the Schmidt number *Sc* and the Brownian motion parameter N*b* cause an increment in the rate of mass transfer whereas opposite effect is noticed for growing values of the thermophoresis motion parameter Nt and the mass stratification parameter Q.

D. The density number

Table V has been presented to portray the effect of the different parameters on the local density number. The results show that gradually mounting values of the buoyancy ratio parameter N*r*, the Eckert number *Ec*, the Schmidt number *Sc* and the bioconvection Lewis parameter *Lb* result an increment in the density number of the motile microorganism whereas reverse situation is observed in case of escalating values of the Rayleigh number *Rb*, the motile density stratification B, the bioconvection Peclet number *Pe* and the microorganism concentration difference parameter Ω.

To analyze the influence of the various parameters on fluid, the dimensionless velocity $f'(\eta)$, the angular velocity $g(\eta)$,

TABLE IV. Numerical values of the local Sherwood number for different parameters when $Pr = Pe = Lb = 1.2$, $Rd = 1$, $\Omega = K = 0.2$, $M = 0.05$, $B = Rb = Nr = \lambda = 0.1$.

S	δ	Ec	Sc	Nt	Nb	Q	$Sh_x Re_x^{-1/2}$
0.1	0.1	0.02	0.2	0.1	0.1	0.1	−0.1501
0.2							−0.1383
0.3							−0.1275
0.1	0.1						−0.1501
	0.2						−0.0768
	0.3						0.0239
	0.1	0.3					−0.1471
		0.4					−0.1460
		0.5					−0.1449
		0.02	0.3				0.0029
			0.4				0.1328
			0.5				0.2460
			0.2	0.3			−1.0517
				0.5			−1.8608
				0.7			−2.5954
				0.1	1		0.2850
					2		0.3111
					3		0.3212
					0.1	0.3	−0.1816
						0.5	−0.2130
						0.7	−0.2440

the dimensionless temperature $\theta(\eta)$, the dimensionless concentration $\phi(\eta)$ and the motile density $\xi(\eta)$ fields are sketched. Fig. 2 is sketched to visualize the variation in the dimensionless velocity $f'(\eta)$ due to changes in the magnetic number M. It is observed that a small increment in the magnetic number

TABLE V. Numerical values of the local density number of the motile microorganism for different parameters when $Pr = Pe = Lb = 1.2$, $\lambda = B = Rb = Nr = Nt = Nb = 0.1$, $Rd = 1$, $M = 0.05$, $\Omega = K = 0.2$.

Nr	Rb	Ec	Sc	Lb	B	Pe	Ω	$Nn_x Re_x^{-1/2}$
0.2	0.1	0.02	0.2	1.2	0.1	1.2	0.2	0.9509
0.3								0.9560
0.4								0.9634
0.2	0.2							0.9520
	0.4							0.9512
	0.6							0.9503
	0.1	0.2						0.9541
		0.4						0.9564
		0.6						0.9587
		0.02	0.4					1.2086
			0.6					1.4164
			0.8					1.5957
			0.2	1				0.8306
				2				1.3561
				3				1.7573
				1.2	0.2			0.9256
					0.3			0.8991
					0.4			0.8725
					0.1	2		0.8489
						3		0.7213
						4		0.5950
						1.2	0.4	0.9235
							0.6	0.8949
							0.8	0.8663

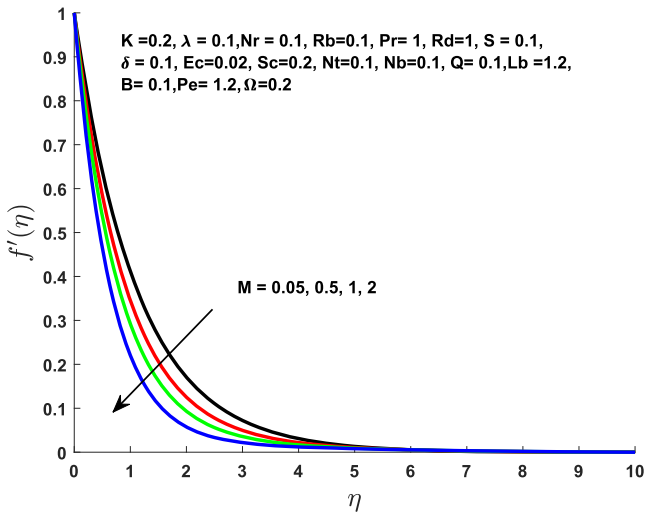

FIG. 2. Effect of M on $f'(\eta)$.

M causes a depreciation in the velocity and its related boundary layer thickness. This verifies the general behavior of the magnetic effect. The velocity field decreases because the drag force is enhanced for with the gradually mounting values of M. From Fig. 3, it is evident that the growing values of the material parameter K enhances the velocity field. As a result the resistance increases, due to which the velocity profile is declined. To study the impact of the mixed convection parameter λ on the velocity profile, Fig. 4 is presented. It is observed that due to gradually mounting values of λ the fluid velocity and related boundary layer thickness is enhanced. It is due to the fact that an enhancement in λ means an enhancement in the buoyancy force due to which the fluid velocity is enhanced. In order to view the impact of the buoyancy ratio parameter Nr on the

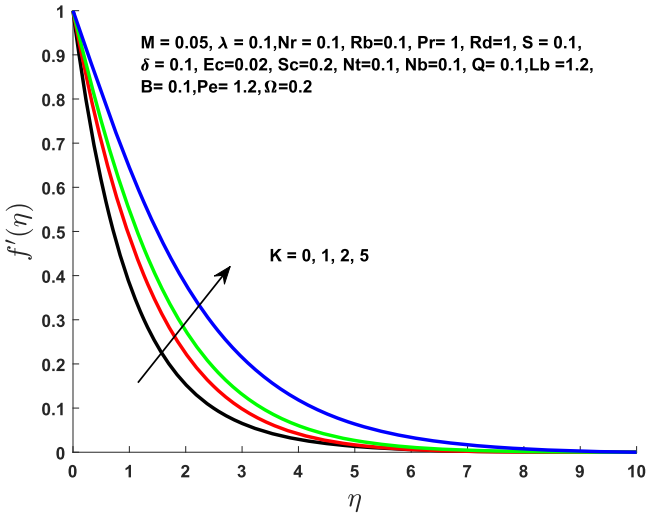

FIG. 3. Effect of K on $f'(\eta)$.

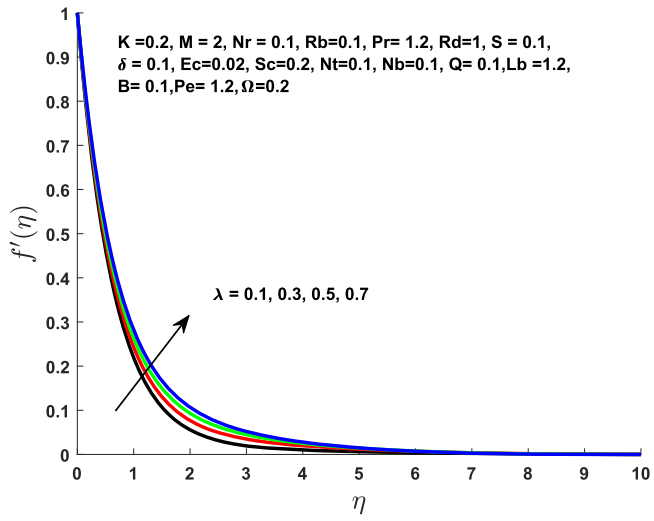

FIG. 4. Effect of λ on $f'(\eta)$.

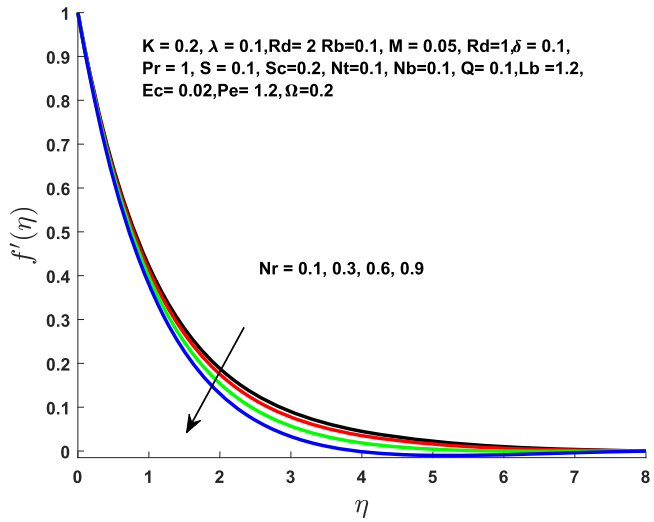

FIG. 5. Effect of *Nr* on $f'(\eta)$.

velocity profile, Fig. 5 is sketched. The dimensionless velocity profile $f'(\eta)$ is declined as *Nr* is increased. The variation in the velocity profile due to an enhancement in the bioconvection Rayleigh number *Rb* can be seen in Fig. 6. An increment in *Rb* increases the buoyancy force due to which the velocity of the fluid is declined. The impact of the thermal stratification parameter *S* on the velocity field $f'(\eta)$ is displayed in Fig. 7. Escalating values of *S* enhances the fluid density in the lower region as compared to the upper region. It results in the reduction in the convective flow between the surface and the ambient flow causing a decrement in the velocity field. Fig. 8 depicts the effect of the material parameter *K* on the angular velocity $g(\eta)$. The curves of this figure indicate that the angular velocity is boosted for the escalating values of *K*. It

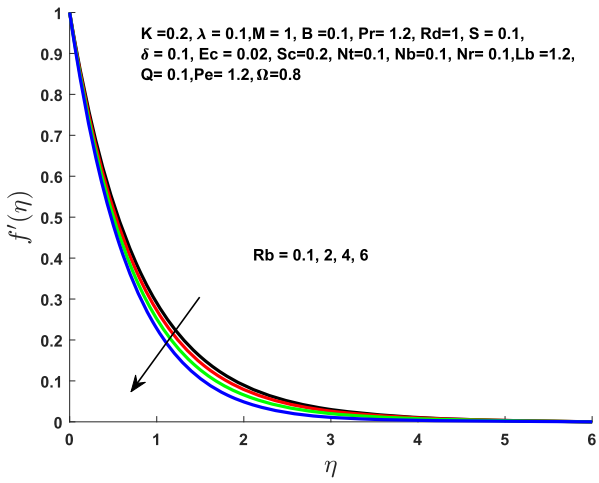

FIG. 6. Effect of *Rb* on $f'(\eta)$.

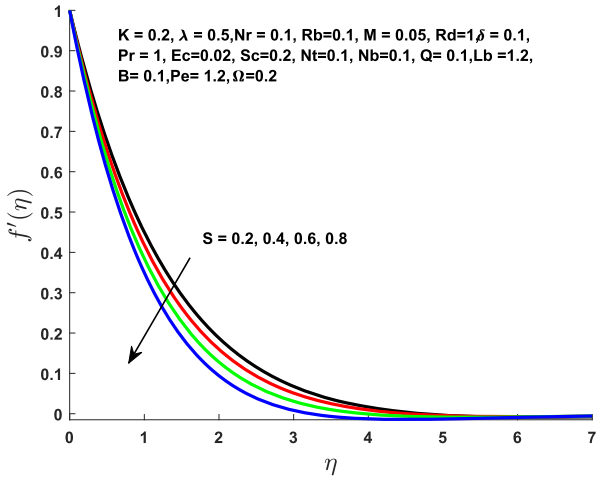

FIG. 7. Effect of *S* on $f'(\eta)$.

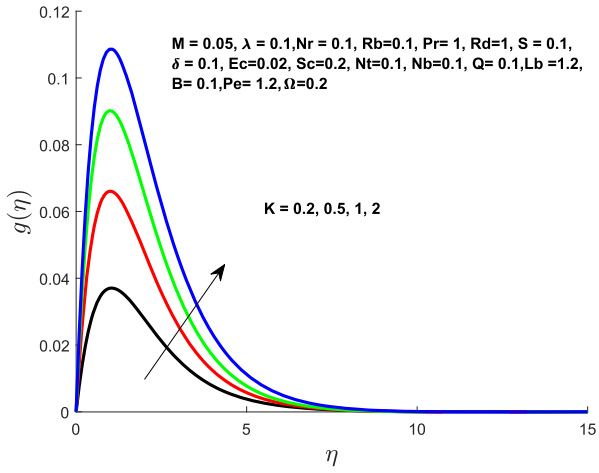

FIG. 8. Effect of *K* on $g(\eta)$.

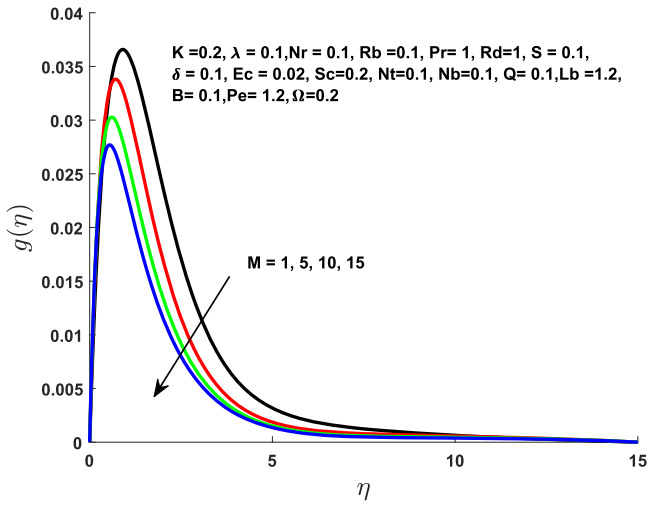

FIG. 9. Effect of M on $g(\eta)$.

is due to the reason that acclivity in the K causes an enhancement in the viscosity of the fluid, due to which the angular velocity is increased. Fig. 9 is displayed to explore the effect of the magnetic number M on the angular velocity $g(\eta)$. The dimensionless angular velocity $g(\eta)$ declines when M is raised. Physically, an increment in the M means an increase in the drag force, which is an opposing force due to which the $g(\eta)$ is decreased.

To study the effect of the various parameters on the dimensionless temperature $\theta(\eta)$, Figs. 10–18 are sketched. The effect of the material parameter K on $\theta(\eta)$ is analyzed in Fig. 10. It is observed that an increment in the material parameter K causes a decrement in $\theta(\eta)$. Fig. 11 indicates the influence of the buoyancy ratio parameter Nr on the dimensionless temperature $\theta(\eta)$. The curves of this figure indicate that an

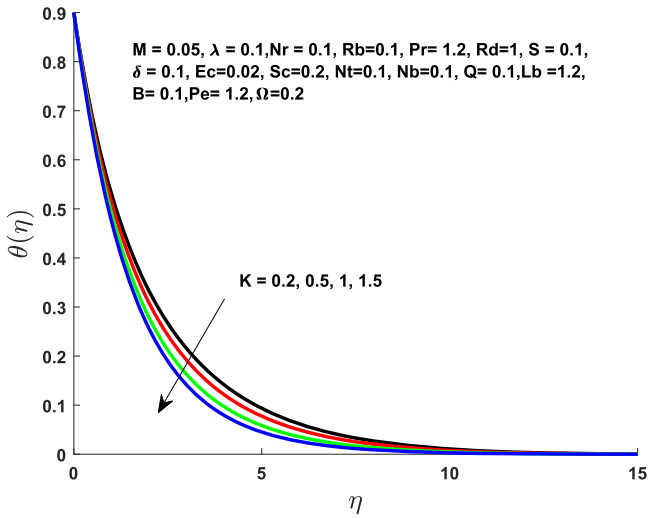

FIG. 10. Effect of K on $\theta(\eta)$.

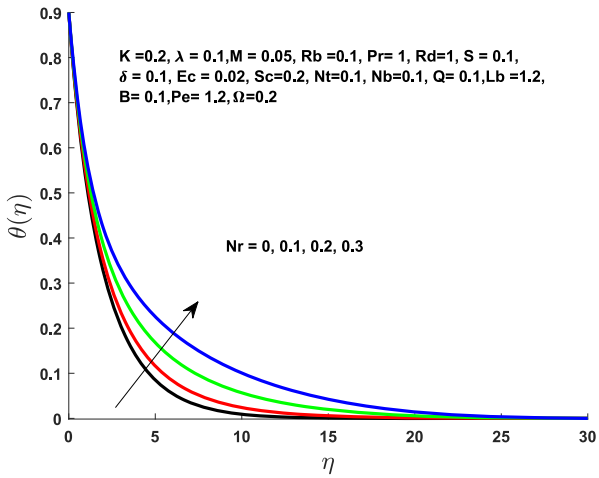

FIG. 11. Effect of Nr on $\theta(\eta)$.

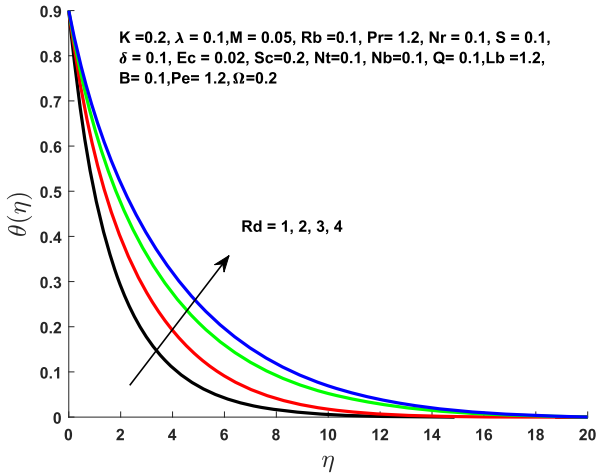

FIG. 12. Effect of Rd on $\theta(\eta)$.

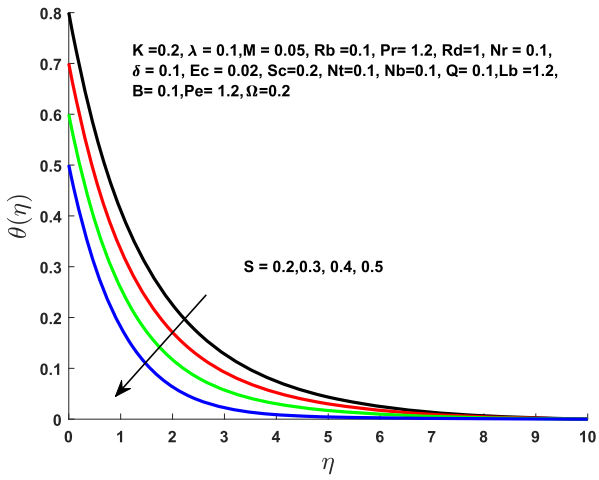

FIG. 13. Effect of S on $\theta(\eta)$.

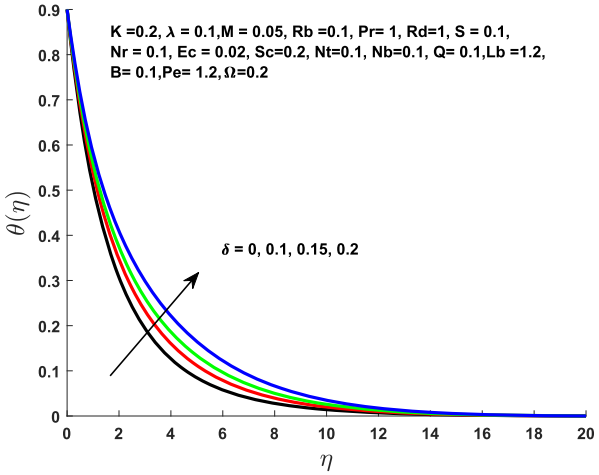

FIG. 14. Effect of δ on $\theta(\eta)$.

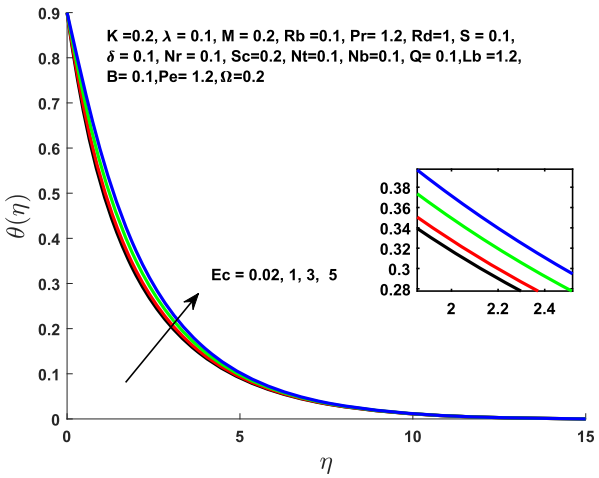

FIG. 15. Effect of *Ec* on $\theta(\eta)$.

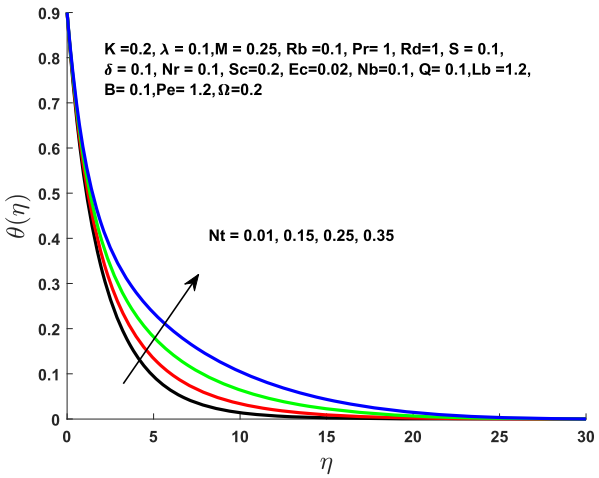

FIG. 16. Effect of *Nt* on $\theta(\eta)$.

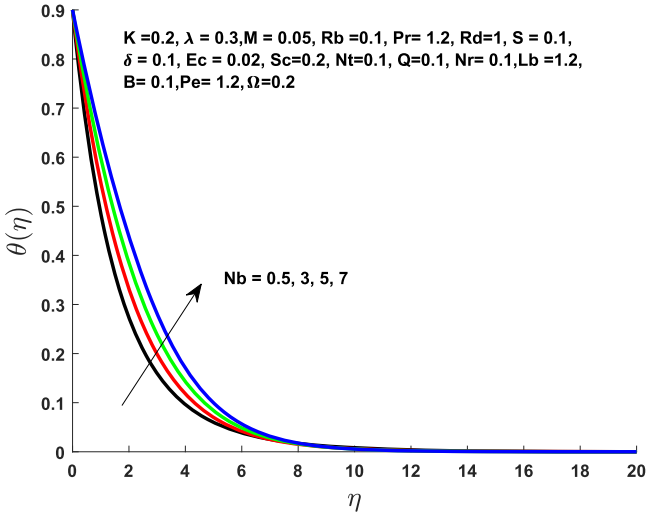

FIG. 17. Effect of *Nb* on $\theta(\eta)$.

increment in parameter Nr increases the $\theta(\eta)$. The dimensionless temperature field $\theta(\eta)$ is increased as the thermal radiation parameter Rd is increased as shown in Fig. 12. Physically, it strengthens the fact that more heat is produced due in the radiation process. The effect of the thermal stratification parameter S on $\theta(\eta)$ is displayed in Fig. 13. An increment in S increases the density of the fluid in the lower region as compared to the upper region. Due to which the temperature difference between the heated surface and away from the surface is declined. It results a reduction in the temperature of the fluid. Fig. 14 depicts the variation in the dimensionless temperature $\theta(\eta)$ due to the heat generation coefficient δ. The dimensionless temperature $\theta(\eta)$ is enhanced

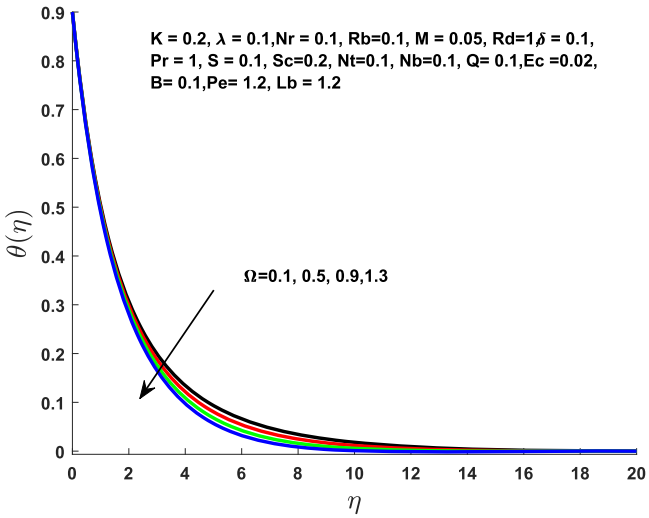

FIG. 18. Effect of Ω on $\theta(\eta)$.

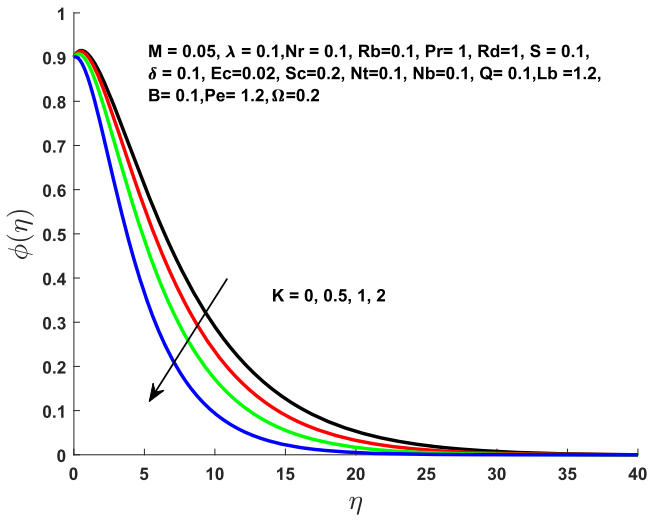

FIG. 19. Effect of K on $\phi(\eta)$.

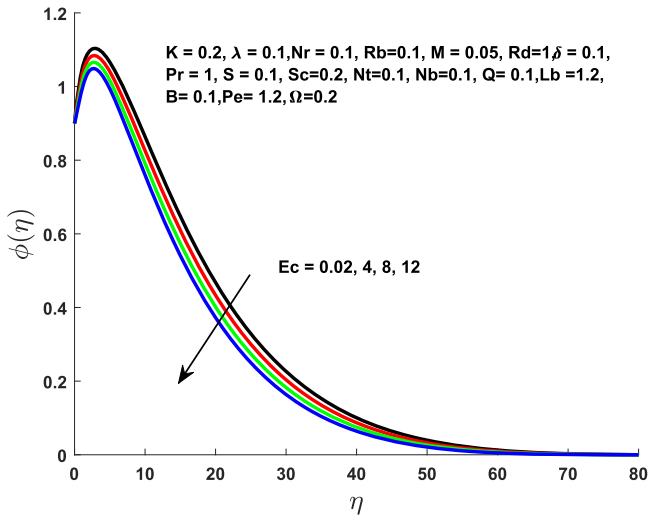

FIG. 21. Effect of Ec on $\phi(\eta)$.

as δ is increased gradually. Physically, the heat source parameter releases energy to the fluid, due to which the temperature of the fluid is enhanced. The effect of the viscous dissipation parameter i.e. the Eckert number Ec on the dimensionless temperature profile $\theta(\eta)$ is visualized in Fig. 15. It is analyzed that an increase in Ec causes an increase in $\theta(\eta)$ and the boundary layer thickness. Physically, the thermal conductivity of the fluid improves as the dissipation increased which helps to enhance the thermal boundary layer thickness. Fig. 16 is drawn to visualize the variation in the dimensionless temperature $\theta(\eta)$ due to the thermophoresis parameter Nt. In this phenomenon, the heated particles are pulled away from hotter region to colder region and so the temperature of the fluid is enhanced. By the Brownian motion theory, the speed of nanoparticles is directly proportional to temperature. With the rises in temperature, the nanoparticles have more kinetic energy yielding, movement faster. Fig. 17 clearly reveals that both the thermal profile and related the boundary layer thickness are raised for the growing values of Nb. In Fig. 18, the impact of the microorganism concentration difference parameter Ω on the dimensionless temperature profile $\theta(\eta)$ is analyzed. It is noticed that the an increment in Ω results a decrement in the energy profile.

To visualize the variation in the dimensionless concentration profile $\phi(\eta)$ due to the emerging physical parameters, Figs. 19–25 are sketched. Fig. 19 is sketched to visualize the variation in concentration profile $\phi(\eta)$ due to changes in the material parameter K. It is noticed that an enhancement in

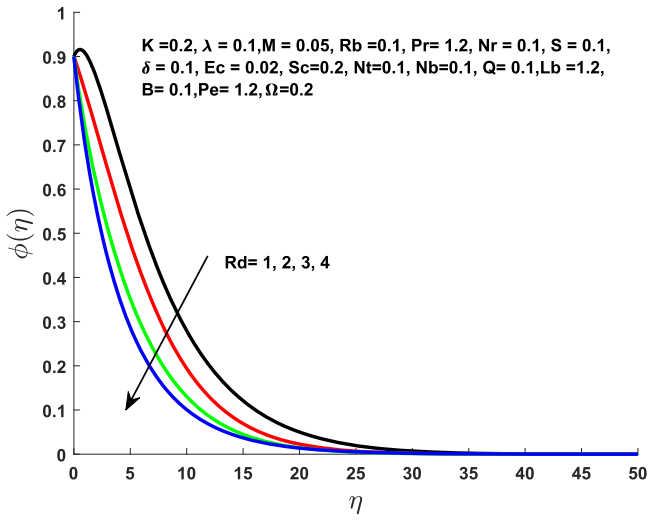

FIG. 20. Effect of Rd on $\phi(\eta)$.

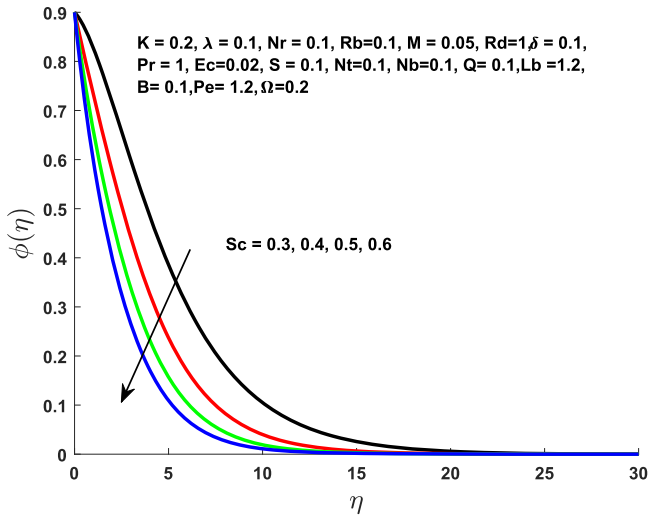

FIG. 22. Effect of Sc on $\phi(\eta)$.

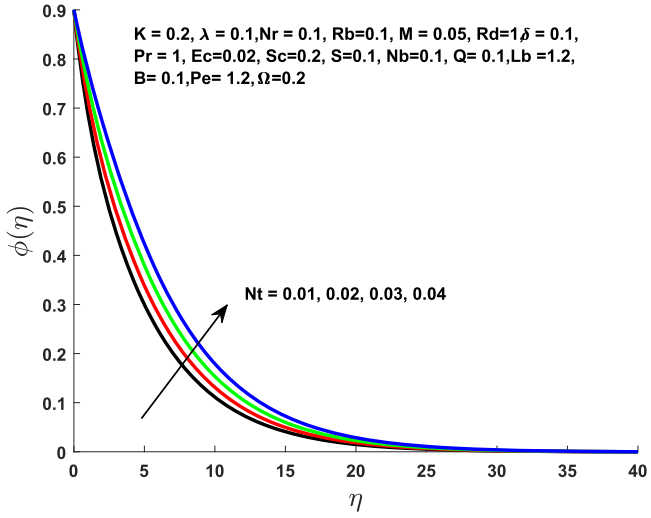

FIG. 23. Effect of *Nt* on $\phi(\eta)$.

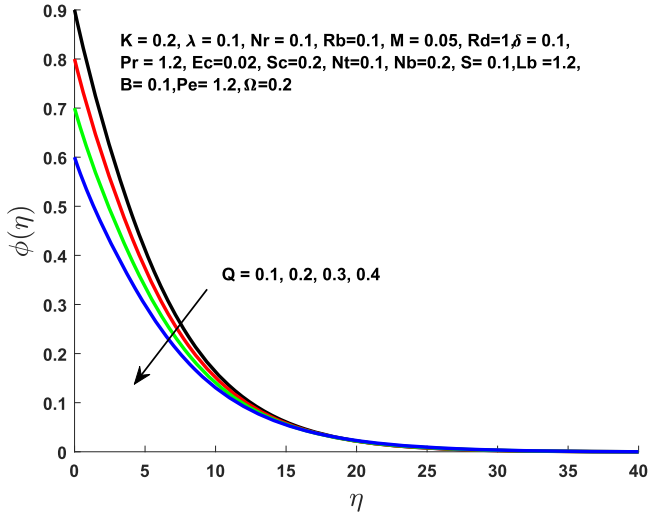

FIG. 25. Effect of *Q* on $\phi(\eta)$.

the *K* results a decrement in $\phi(\eta)$. Fig. 20 illustrates the effect of the thermal radiation parameter *Rd* on the dimensionless concentration profile $\phi(\eta)$. Graphs of this figure indicate that $\phi(\eta)$ is reduced as *Rd* is hiked. Fig. 21 is prepared to inspect the impact of the Eckert number *Ec* on the concentration profile $\phi(\eta)$ which shows that an enhancement in *Ec* results a decline in $\phi(\eta)$. Fig. 22 is sketched to present the effect of the Schmidt number *Sc* on the dimensionless concentration profile $\phi(\eta)$. For the boosting values of *Sc*, $\phi(\eta)$ is enhanced. It is due to the fact that the mass diffusivity has inverse relation with the Schmidt number therefore the higher values of Schmidt number brings weaker mass diffusion as a result nanoparticles concentration is dropped. The impact of the thermophoresis parameter *Nt* on the concentration profile $\phi(\eta)$ is presented in Fig. 23. These curves show that $\phi(\eta)$ is an increasing function of *Nt*. Fig. 24 is prepared to visualize the impact of the Brownian motion parameter *Nb* on $\phi(\eta)$. An acclivity in *Nb* causes a decrement in $\phi(\eta)$. Physically, the Brownian motion heats up the fluid in the boundary layer and also aggravates the particles away from the fluid regime, therefore a decrement is seen in the concentration profile. The influence of the mass stratification parameter Q is displayed in Fig. 25. An increment in Q reduces the $\phi(\eta)$ and the related boundary layer thickness.

The variations in the motile density profile $\xi(\eta)$ due to different involved parameters is presented in the Figs. 26–37. The impact of the material parameter *K*, on the motile

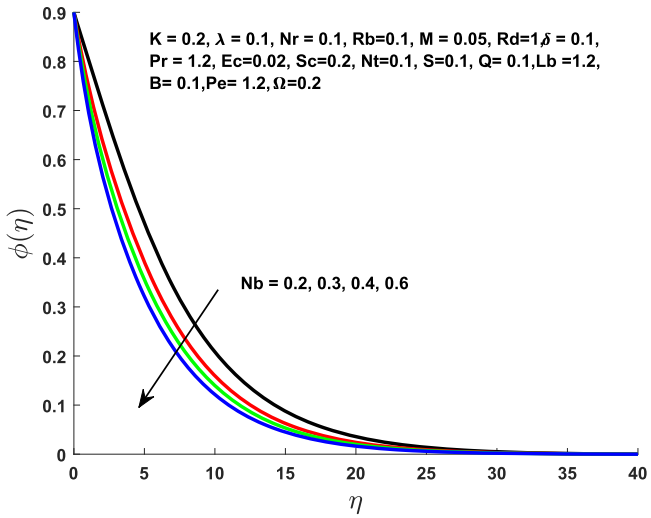

FIG. 24. Effect of *Nb* on $\phi(\eta)$.

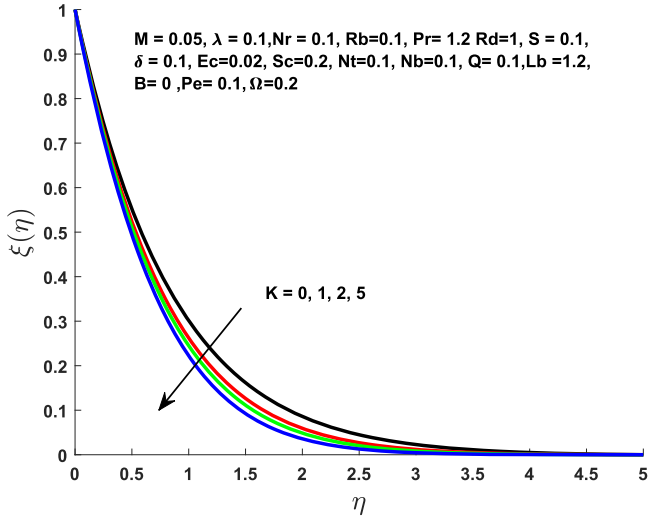

FIG. 26. Effect of *K* on $\xi(\eta)$.

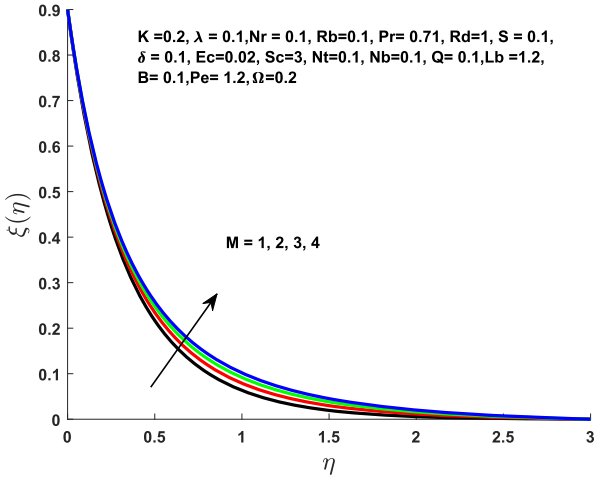

FIG. 27. Effect of M on $\xi(\eta)$.

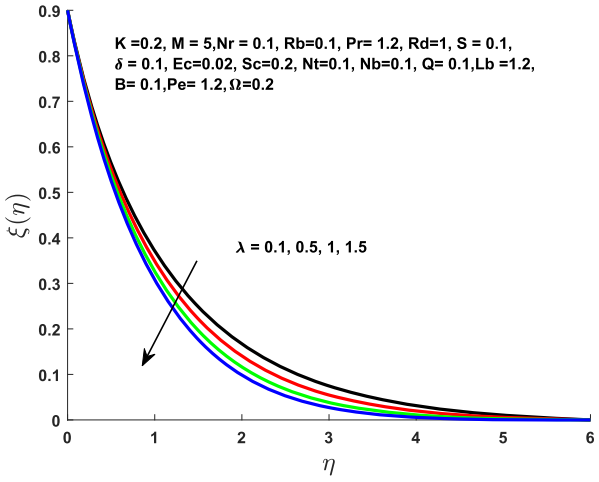

FIG. 28. Effect of λ on $\xi(\eta)$.

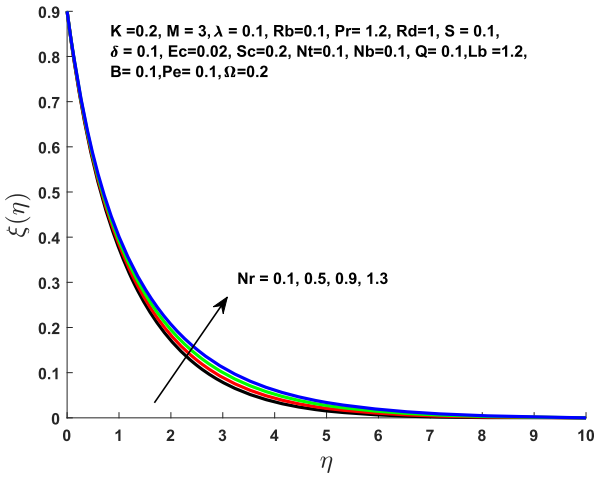

FIG. 29. Effect of Nr on $\xi(\eta)$.

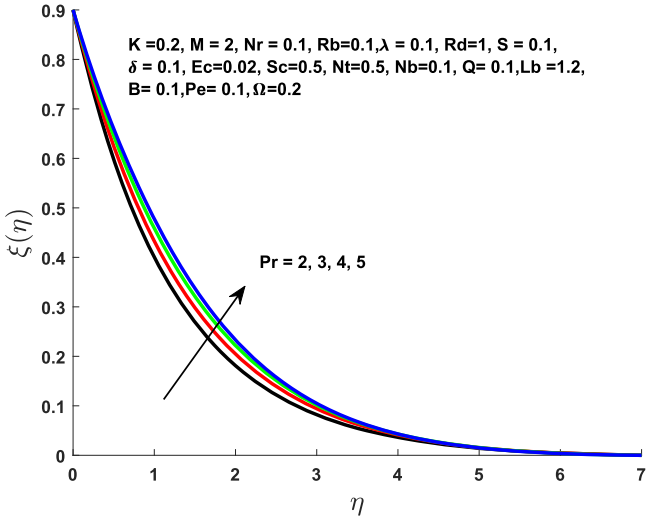

FIG. 30. Effect of Pr on $\xi(\eta)$.

density profile $\xi(\eta)$ is illustrated in Fig. 26. As expected, due to an increase in the material parameter K the motile density profile $\xi(\eta)$ is decreased. Fig. 27 is aimed to analyze the motile density profile $\xi(\eta)$ for the increasing values of the magnetic number M. These curves reflect that an increment in M results an enhancement in the motile density profile $\xi(\eta)$. The impact of the mixed convection parameter λ on the motile density profile $\xi(\eta)$ is reported in the Fig. 28. The motile density profile $\xi(\eta)$ is a decreasing function of λ. As λ is the ratio of the buoyancy force to the viscous force, therefore an increment in λ causes a decrement in the motile density. Fig. 29 is plotted to visualize the variation in motile density profile $\xi(\eta)$ due to the buoyancy ratio parameter Nr. An increment in Nr increases the motile density profile $\xi(\eta)$. It is due to the fact that Nr

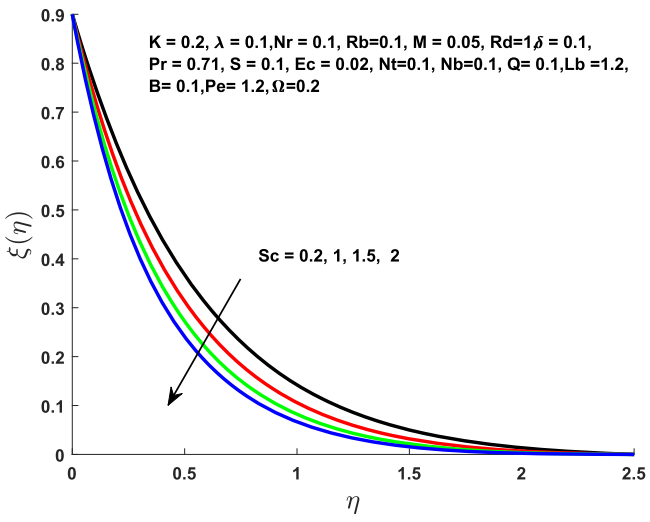

FIG. 31. Effect of Sc on $\xi(\eta)$.

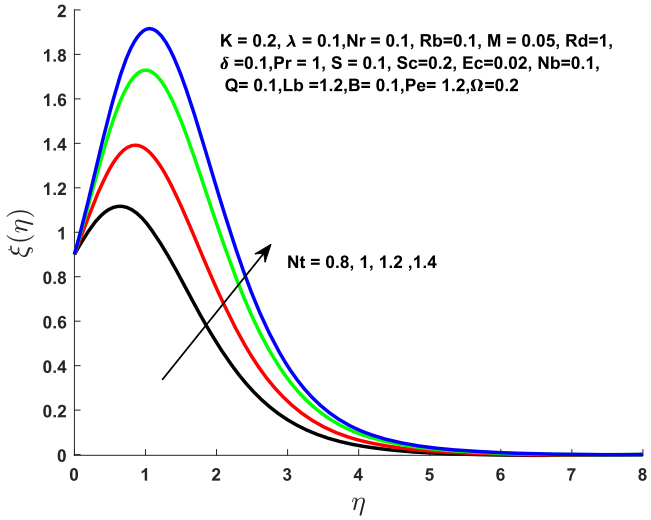

FIG. 32. Effect of *Nt* on $\xi(\eta)$.

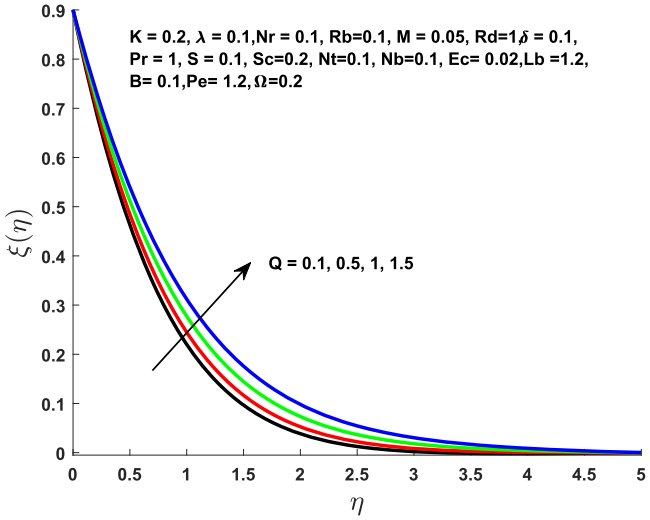

FIG. 34. Effect of *Q* on $\xi(\eta)$.

increases the solutal buoyancy force due to which the fluid density is increased. To analyze the effect of the Prandtl number *Pr* on the motile density profile $\xi(\eta)$, Fig. 30 is prepared. Both the motile density profile and the related boundary layer thickness are enhanced. Fig. 31 is sketched to present the effect of the Schmidt number *Sc* on the motile density profile $\xi(\eta)$. The motile density profile $\xi(\eta)$ is declined for boosting values of Sc. Fig. 32 is prepared to visualize the effect of the thermophoresis parameter *Nt* on the motile density profile $\xi(\eta)$. An acclivity in *Nt* causes an increment in the motile density profile $\xi(\eta)$. To visualize the effect of *Nb* on motile density profile $\xi(\eta)$, Fig. 33 is sketched. An increment in the parameter *Nb* means an increment in the random motion of the fluid particles due to which the motile density of the fluid is decreased. The gradually mounting values of the mass stratification parameter Q causes an increment in the motile density profile $\xi(\eta)$ as shown in the Fig. 34. It is due to the reason that an increment in the parameter Q decreases the concentration difference of the nanoparticles between the surface and away from the surface. The motile density profile $\xi(\eta)$ is a decreasing function of the bioconvection Lewis number *Lb* as shown in the Fig. 35. The higher values of the *Lb* means a decrement in the diffusivity of the motile microorganism and thus $\xi(\eta)$ is diminished. The effect of the motile density stratification *B* on the motile density profile $\xi(\eta)$ is illustrated in the Fig. 36. The acclivity in the motile density stratification *B* reduces the motile density profile $\xi(\eta)$. Physically, it is due to the decrease in the concentration difference of the microorganism between

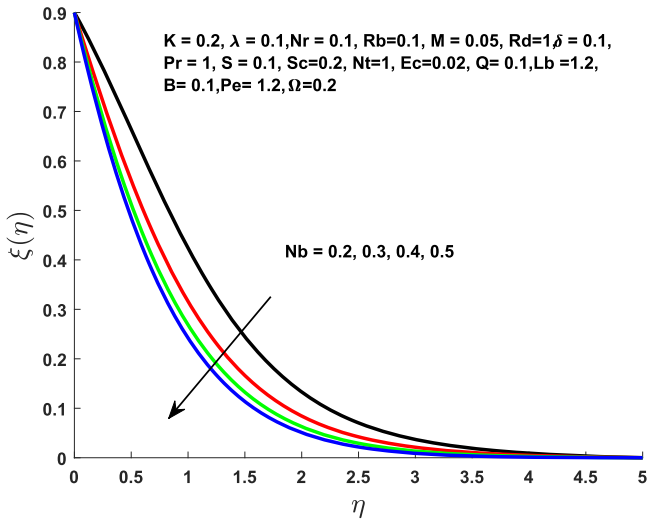

FIG. 33. Effect of *Nb* on $\xi(\eta)$.

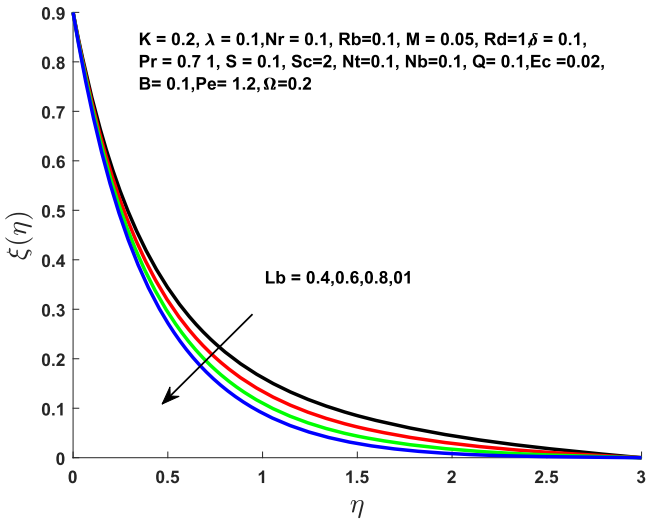

FIG. 35. Effect of *Lb* on $\xi(\eta)$.

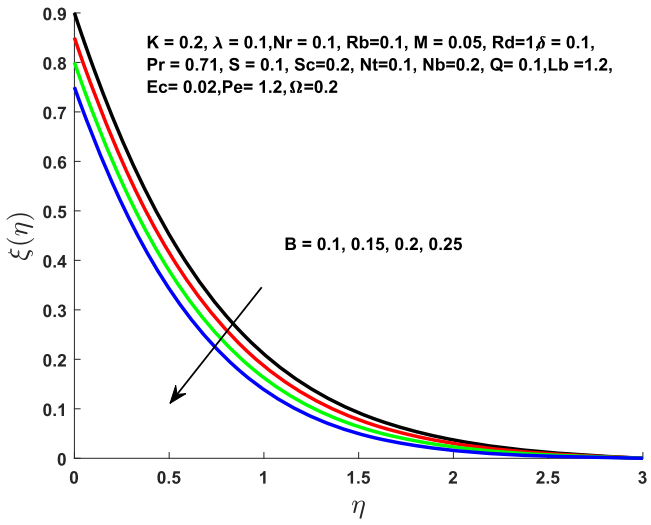

FIG. 36. Effect of B on $\xi(\eta)$.

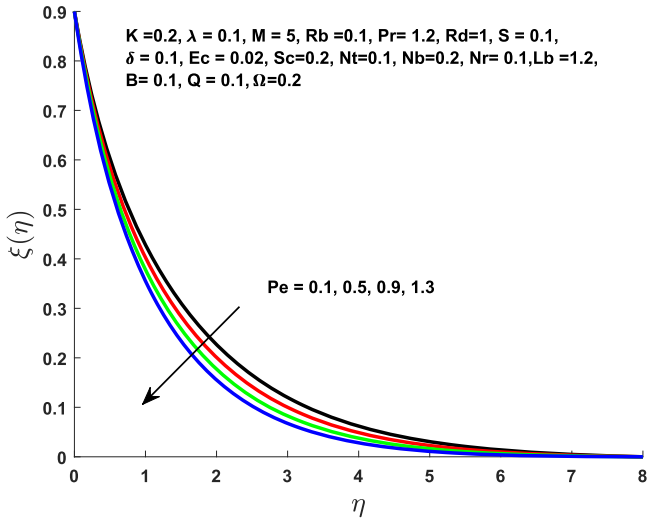

FIG. 37. Effect of Pe on $\xi(\eta)$.

the surface and away the surface. The motile density profile $\xi(\eta)$ is decreased for growing values of the Peclet number Pe as represented in Fig. 37. Gradually mounting values of Pe result a decrement in the diffusivity of the microorganism due to which the motile density profile is diminished. It is due to the fact that an increment in the Peclet number yields the enhancement in the motion of fluid particles which cause the reduction in thickness of motile microorganisms.

V. FINAL REMARKS

In this article two dimensional magnetohydrodynamic micropolar nanofluid with gyrotactic microorganism has been analyzed. Some of the key findings have been summarized as below:

- Both the velocity and the angular velocity is increased for the large value of the material parameter K, but a decrement is noticed for the gradually mounting values of the magnetic number M.
- The energy profile is enhanced for an acclivity in the buoyancy ratio parameter Nr and the thermal radiation parameter Rd.
- A decrement in the concentration profile is observed for an acclivity in the material parameter K, the Schmidt number Sc and the mass stratification parameter Q.
- The density profile is enhanced for the enhancement in each of the mass stratification parameter Q and the buoyancy ratio parameter Nr.
- The temperature profile is diminished the thermal stratification parameter S and the material parameter K.
- The density profile is reduced for an enhancement in the material parameter K, the Peclet number Pe, the bioconvection Lewis parameter Lb, the motile density stratification B and the mixed convection parameter λ.

REFERENCES

[1]L. Zheng, J. Niu, X. Zhang, and Y. Gao, "MHD flow and heat transfer over a porous shrinking surface with velocity slip and temperature jump," International Journal of Biomathematics **56**(5-6), 133–144 (2012).

[2]D. S. Chauhan and R. Agrawal, "MHD flow and heat transfer in a channel bounded by a shrinking sheet and a porous medium bed," International Scholarly Research Notices **2013**.

[3]H. A. Attia, "Unsteady MHD Couette flow and heat transfer of dusty fluid with variable physical properties," Applied Mathematics and Computation **177**(1), 308–318 (2006).

[4]K. G. Kumar, M. Archana, B. J. Gireesha, M. R. Krishanamurthy, and N. G. Rudraswamy, "Cross diffusion effect on MHD mixed convection flow of nonlinear radiative heat and mass transfer of Casson fluid over a vertical plate," Results in Physics **8**, 694–701 (2018).

[5]A. C. Eringen, "Theory of micropolar fluids," International Journal of Mathematics and Mechanics **16**, 1–18 (1966).

[6]A. C. Eringen, "Theory of thermomicrofluids," Journal of Mathematical Analysis and Applications **38**(2), 480–496 (1972).

[7]V. M. Soundalgekar and H. S. Takhar, "Flow of micropolar fluid past a continuously moving plate," International Journal of Engineering Science **21**(8), 961–965 (1983).

[8]N. Eldabe and M. E. M. Ouaf, "Chebyshev finite difference method for heat and mass transfer in a hydromagnetic flow of a micropolar fluid past a stretching surface with Ohmic heating and viscous dissipation," Applied Mathematics and Computation **177**(2), 561–571 (2006).

[9]S. S. Motsa and S. Shateyi, "The effects of chemical reaction, Hall and ion-slip currents on MHD micropolar fluid flow with thermal diffusivity using a novel numerical technique," Journal of Applied Mathematics **2012**.

[10]M. Bilal, S. Hussain, and M. Sagheer, "Boundary layer flow of magneto-micropolar nanofluid flow with Hall and ion-slip effects using variable thermal diffusivity," Bulletin of the Polish Academy of Sciences **65**(3) (2017).

[11]K. L. Hsiao, "Micropolar nanofluid flow with MHD and viscous dissipation effects towards a stretching sheet with multimedia feature," International Journal of Heat and Mass Transfer **112**, 983–990 (2017).

[12]S. M. Atif, S. Hussain, and M. Sagheer, "Numerical study of MHD micropolar Carreau nanofluid in the presence of induced magnetic field," AIP Advances **8**, 035219 (2018).

[13]S. U. S. Choi and J. A. Eastman, "Enhancing thermal conductivity of fluids with nanoparticles," ASME Fluids Engineering **231**, 99–105 (1995).
[14]M. M. Rashidi, Z. Yang, M. Awais, M. Nawaz, and T. Hayat, "Generalized magnetic field effects in Burgers nanofluid model," PLoS One **2**(1), e0168923 (2017).
[15]Y. Feng and C. Kleinstreuer, "Nanofluid convective heat transfer in a parallel-disk system," International Journal of Heat and Mass Transfer **53**(21-22), 4619–4628 (2010).
[16]G. J. Reddy, M. Kumar, B. Kethireddy, and A. Chamka, "Colloidal study of unsteady magnetohydrodynamic couple stress fluid flow over an isothermal vertical flat plate with entropy heat generation," Journal of Molecular Liquids **253**, 169–179 (2018).
[17]S. Bhattacharyya and S. K. Pal, "Enhanced electroosmotic flow in a nanochannel patterned with curved hydrophobic strips," Applied Mathematical Modelling **54**, 567–579 (2018).
[18]A. V. Kuznetsov, "Bio-thermal convection induced by two different species of microorganisms," International Communications in Heat and Mass Transfer. **38**, 548–553 (2011).
[19]A. V. Kuznetsov, "The onset of nanofluid bioconvection in a suspension containing both nanoparticles and gyrotactic microorganisms," International Communications in Heat and Mass Transfer **37**, 1421–1425 (2010).
[20]A. V. Kuznetsov, "Nanofluid bioconvection in porous media: Oxytactic microorganisms," Journal of Porous Media **15**, 233–248 (2012).
[21]H. Xu and I. Pop, "Fully developed mixed convection flow in a horizontal channel filled by a nanofluid containing both nanoparticles and gyrotactic microorganisms," European Journal of Mechanics - B/Fluids **46**, 37–45 (2014).
[22]C. S. K. Raju and N. Sandeep, "Heat and mass transfer in MHD non-Newtonian bio-convection flow over a rotating cone/plate with cross diffusion," Journal of Molecular Liquids **215**, 115–126 (2016).
[23]L. Wang and J. Fan, "Nanofluids research: Key issues," Nanoscale Reserch Letters **5**, 1241–1252 (2010).
[24]E. Ramya, M. Muthtamiselan, and D. H. Doh, "Absorbing/emitting radiation and slanted hydromagnetic effects on micropolar liquid containing gyrostatic microorganisms," Applied Mathematics and Computation **324**, 69–81 (2018).
[25]A. Ishak, "Thermal boundary layer flow over a stretching sheet in a micropolar fluid with radiation effect," Meccanica **45**(3), 367–373 (2010).
[26]T. Sajid, M. Sagheer, S. Hussain, and M. Bilal, "Darcy-Forchheimer flow of Maxwell nanofluid flow with nonlinear thermal radiation and activation energy," AIP Advances **8**, 035102 (2018).
[27]S. M. Atif, S. Hussain, and M. Sagheer, "Effect of thermal radiation and variable thermal conductivity on magnetohydrodynamics squeezed flow of Carreau fluid over a sensor surface," Journal of Nanofluid **8**, 806–816 (2019).
[28]T. Y. Na, *Computational methods in engineering boundary value problems* (Academic Press, 1979), pp. 71–76.